Electron capture by fast protons in Ar: Cross sections for capture from the M shell

E. Horsdal Pedersen and J. P. Giese*
Institute of Physics, University of Aarhus, DK-8000 Aarhus C, Denmark
(Received 5 December 1989)

Charge-state distributions of slow recoil ions produced in the single-electron-capture reaction $H^+ + Ar \rightarrow H + Ar^{q+}$ have been measured in the energy range 800–3500 keV to supplement and confirm previous measurements in the energy range 500–1750 keV. The observed singly charged recoil ions, Ar^+, originate almost exclusively from capture in the M shell. The M-shell-capture cross section deduced from the measured fractions of Ar^+ ions and well-established total-capture cross sections taken from the literature exhibits a pronounced structure. It is suggested that this structure is due to one or two radial nodes of the wave functions that describe the M shell.

I. INTRODUCTION

DuBois and Manson[1] recently reviewed the experimental work on ionization in proton-atom collisions. In the discussion, the authors draw attention to the cross section for single ionization of Ar by electron capture, $H^+ + Ar \rightarrow H + Ar^+$, and point out that there is a sudden change in the energy dependence of the cross section near a projectile energy E of 450 keV. The change is from $E^{-4.8}$ for E between 150 and 400 keV to $E^{-3.1}$ for E above 500 keV. This apparent anomaly was tentatively explained as a shell effect. At energies below 450 keV, the cross section is dominated by capture from the outermost shell which is the M shell. At higher energies, capture from an inner shell, followed by radiative decay, could conceivably account for the observed structure. The explanation is supported by experimental L-shell-capture cross sections[2] which show that capture from the L shell is the dominant capture channel at energies above approximately 500 keV. However, for this model to give quantitative agreement with the observations,[1] the fluorescence yields for the Ar L subshells would have to be more than a factor of 10 higher than currently accepted.[3,4] As a consequence, the anomaly or structure was left unexplained. A similar structure was seen for Kr but not for He and Ne.

There is actually no reason to expect that the electron-capture cross section for a given shell should decrease smoothly without structure when the energy is increased. This is demonstrated theoretically for the higher shells of Ar and Kr (Refs. 5 and 6) and for excited states of H.[7,8] For these initial states, the calculations indeed show structures which, although this is not stated explicitly in the articles, may be traced to the nodal structure of the wave functions used.

The cross section for the reaction $H^+ + Ar \rightarrow H + Ar^+$, which we are concerned with here, was deduced[1] from recoil charge-state distributions measured in only one experiment.[9] The present effort is a repetition and extension of this experiment under improved experimental conditions to confirm and supplement the original data. We argue that the structure, which was found previously[1] and which has been confirmed in the present experiment, is caused by radial nodes of the $3s$ and $3p$ wave functions of the Ar atom. To the best of our knowledge, this is the first time that such a structure has been observed experimentally for charge transfer.

II. EXPERIMENT

A schematic diagram of the experimental arrangement is shown in Fig. 1. The mass-analyzed beam from the accelerator (5-MV single-stage Van de Graaff with rf ion source) was collimated by two sets of adjustable slits C set typically at 0.1×0.1 mm^2 or less and separated by about 2000 mm. The magnetic field B directed the collimated proton beam into the differentially pumped target-gas cell G, with 1 and 2 mm entrance and exit apertures, respectively. Slow recoil ions were extracted electrostatically from the gas cell by an extraction system E, consisting of a number of acceleration electrodes and a set of electrostatic deflection plates. The extraction field in the gas cell was about 600 V/cm, and the total extraction voltage was typically 4 kV, resulting in recoil-ion energies of 4, 8 keV, etc., depending on the charge state of the recoil ion. The potential of one of the electrodes close to the gas cell is variable, making it possible to adjust the focusing properties of the extraction system. Electrostatic deflection plates allow the extracted ions to be steered. The extraction system is purely electrostatic. Therefore ions of different charge state follow the same trajectory. A magnetic field B provided by a permanent magnet separates the charge states before detection by a ceramic channeltron capable of counting up to 20,000 particles/s with only a small change of gain.

After passing through the gas cell, the beam particles were charge-state analyzed by the electrostatic deflector D. The protons were stopped by an insulated plate S, also used for beam-current measurements. The H atoms formed in capture reactions in the gas cell were counted by a surface-barrier detector(SB), with a sensitive area of 300 mm^2 situated about 2000 mm from the gas cell. The detector covered scattering angles up to 5 mrad, which is large enough to detect essentially all of the scattered H atoms at the high beam velocities used in this experiment.

The electronics consisted of fast amplifiers on both

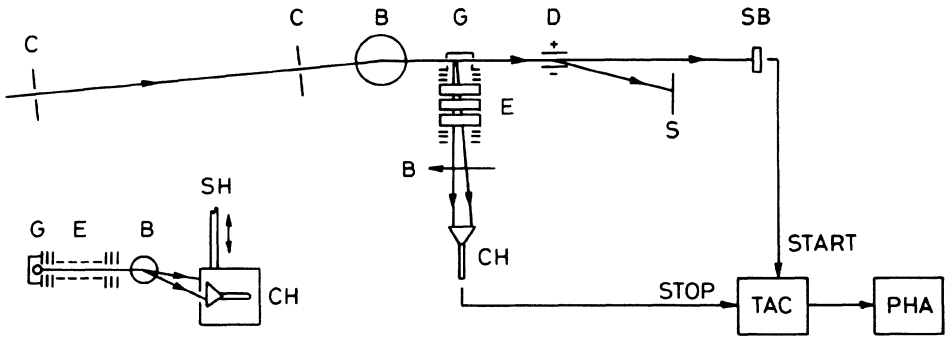

FIG. 1. Experimental arrangement. *C*, collimators; *B*, magnetic fields; *G*, gas cell; *E*, recoil-ion extraction system; *D*, electrostatic deflectors; *S*, beam stop; SB, surface-barrier detector; and CH, ceramic channeltron. Electronics: TAC, time-to-amplitude converter; and PHA, pulse-height analyzer. SH, shaft attached to computer-controlled micrometer screw.

branches shown in Fig. 1, CAMAC scalers for the singles events, a time-to-amplitude converter (TAC), and a pulse-height analyzer (PHA), to identify coincident events, and a step-motor setting the position of the channeltron (CH), via a micrometer screw attached to the shaft (SH). The step motor and the data-acquisition system were controlled by a computer which also did most of the data reduction on-line.

An example of primary experimental data is shown in Fig. 2. One axis shows the time correlation between start and stop pulses, as measured by the TAC. The other shows the position of the channeltron CH. The peaks in the time spectra show the coincident events. Due to the different acceleration of ions of different charge states, the time correlation alone identifies the charge state of the extracted ion. Therefore no further separation of charge states is necessary in principle. However, due to the overwhelming dominance among the extracted ions of singly charged particles from pure-ionization events, which are not in coincidence, it is advantageous to separate the charge states spatially. By avoiding the high uncorrelated count rate from these singly charged ions, acceptable reals-to-random ratios for the highly charged recoil ions were obtained. In practice, recoil charge states 1, 2, and 3 were measured in one run, with the beam intensity limited by the capability of the channeltron CH, whereafter charge states 3, 4, and 5 were measured in another run with higher beam intensity.

Coincident charge-state distributions are shown in Fig. 3. Charge states 2 and 3 dominate. This shows that capture from the various inner subshells, with subsequent Coster-Kronig and Auger decays, are the most important capture channels at this particular energy (2.5 MeV). The charge states are not fully separated by the magnetic

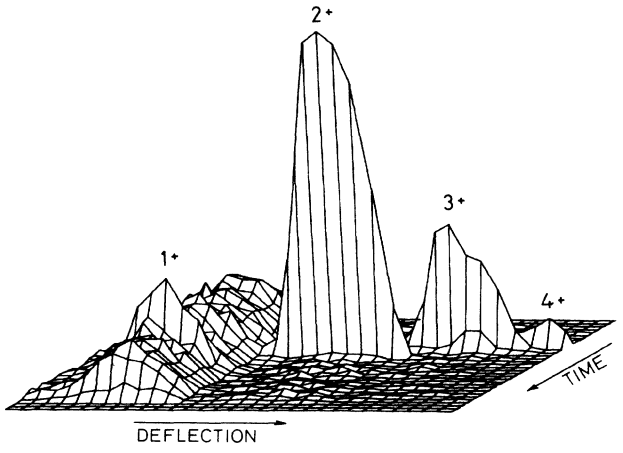

FIG. 2. Three-dimensional plot showing the contents of the two-dimensional spectrum, holding the recoil-ion charge-state data obtained for 2.5-MeV protons on Ar. One axis shows the time correlation between start and stop pulses and the other the deflection in the magnetic field (see Fig. 1). The peaks show coincidences with recoil-ion charge states 1–4.

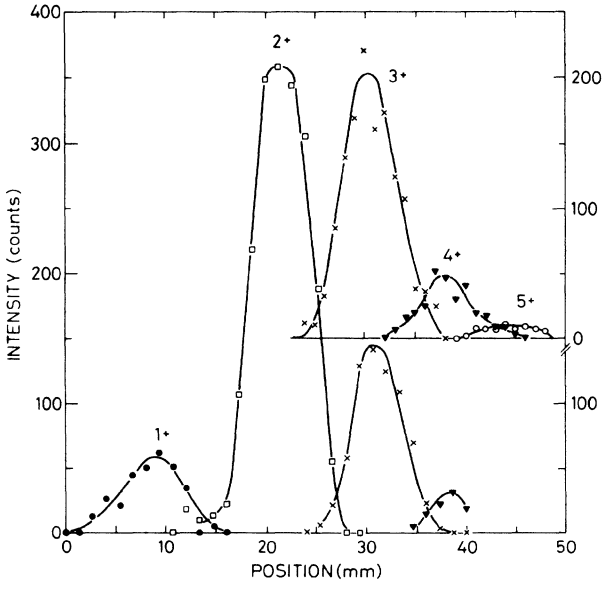

FIG. 3. Charge-state distribution of Ar recoil ions produced in single-electron-capture reactions by 2.5-MeV protons. Charge states 1, 2, 3, and partly 4 were usually measured in one run (see Fig. 2), and charge states 3, 4, and 5 in a separate run. The zero point of the detector position is arbitrary.

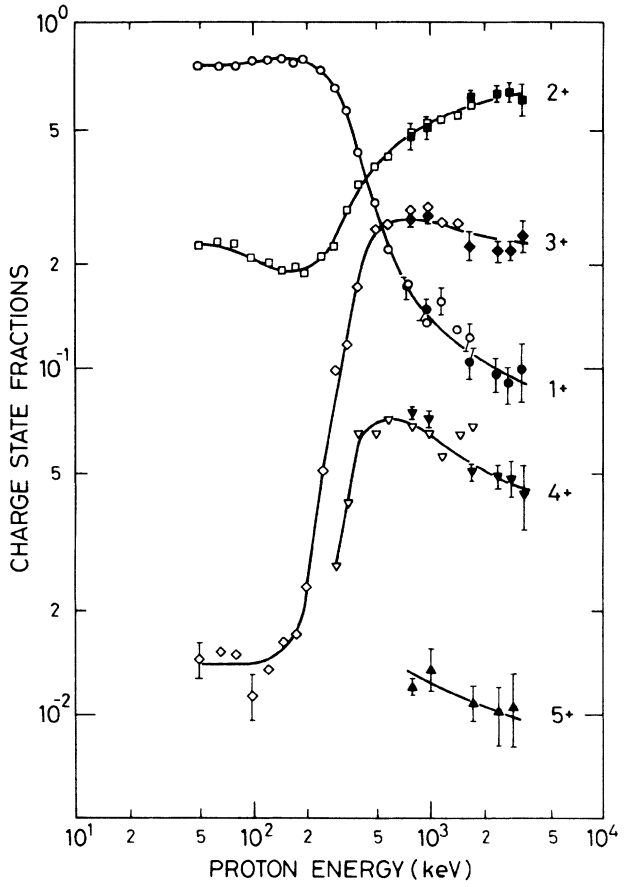

FIG. 4. Energy dependence of charge-state distributions of Ar recoil ions produced in single-electron-capture reactions by protons. The open symbols show the previous data (Ref. 9) and the closed symbols the presented data.

analyzer, but the combined dispersion in space and time provides excellent separation.

Recoil-ion charge-state distributions were measured at several pressures to ensure that the distributions are independent of pressure. The precise target thickness was not measured, but an upper limit of 10^{13} atoms/cm^2 was estimated.

III. EXPERIMENTAL RESULTS AND DISCUSSION

The measured charge-state distributions of slow recoil ions in coincidence with single capture are plotted in Fig. 4. The error bars indicate statistical standard deviations estimated on the basis of counting statistics, including the correction for random coincidence. The data are compared with distributions measured in a previous experiment,[9] using a different experimental arrangement which did not provide spatial separation of the recoil charge states. The agreement between the two sets of data is excellent. The extension of the energy range covered from 50–1750 keV to 50–3500 keV was possible only due to the spatial separation of the recoil charge states, which greatly improved the conditions for unambiguously identifying the coincidences with highly charged recoil ions.

The cross section for single ionization by capture, $H^+ + Ar \rightarrow H + Ar^+$, was found by multiplying total-capture cross sections[10] by the fraction of singly charged recoil ions produced in the reaction. This cross section is due almost exclusively to capture from the M shell because capture from the L shell leads to multiple ionization via Auger and Coster-Kronig transitions with almost 100% probability. It should be realized, however, that the derived cross section does not include all capture events from the M shell. M-shell capture can be accompanied by simultaneous ionization of other electrons by the projectile or by shakeoff due to the adjustment of the remaining electrons, subsequent to the sudden removal of one M-shell electron. The experimental condition on the cross section, that only the single ionization inherent in the capture process is included, makes the measured cross section smaller than the unrestricted M-shell-capture cross section. The shakeoff probability is of the order of 15% and should not depend appreciably on energy within the energy range of interest here. The probability of direct ionization simultaneously with another inelastic process may be estimated from the measured sin-

TABLE I. For the reaction $p + Ar \rightarrow H + Ar^{q+}$, we list proton energy, E, fraction of recoil ions with $q = 1$, F_{1+}, total electron-capture cross section, σ_C^{tot} (Ref. 10), and cross section for capture from the M shell, σ_C^M. The upper part of the table lists the previous data (Ref. 9) and the lower part the new data, including statistical standard deviations for F_{1+}. $x[y] = x \times 10^y$.

E (keV)	F_{1+} (%)	σ_C^{tot} (cm^2)	σ_C^M (cm^2)
50	75.8	3.2[−16]	2.4[−16]
65	75.1	2.6[−16]	2.0[−16]
80	75.5	1.6[−16]	1.2[−16]
100	77.8	1.1[−16]	8.6[−17]
125	78.3	6.5[−17]	5.1[−17]
150	79.0	3.7[−17]	2.9[−17]
175	77.5	2.1[−17]	1.6[−17]
200	78.5	1.1[−17]	8.6[−18]
250	74.0	2.5[−18]	1.9[−18]
300	65.0	9.7[−19]	6.3[−19]
350	55.7	7.5[−19]	4.2[−19]
400	42.2	4.6[−19]	1.9[−19]
500	30.2	3.4[−19]	1.0[−19]
600	22.2	2.3[−19]	5.1[−20]
800	17.6	1.3[−19]	2.3[−20]
1000	13.7	7.3[−20]	1.0[−20]
1200	15.8	4.5[−20]	7.1[−21]
1500	13.1	2.4[−20]	3.1[−21]
1750	12.4	1.6[−20]	2.0[−21]
800	17.3±1.0	1.3[−19]	2.2[−20]
1000	14.9±1.0	7.3[−20]	1.1[−20]
1750	10.5±1.1	1.6[−20]	1.7[−21]
2500	9.7±1.1	5.3[−21]	5.1[−22]
3000	9.1±1.1	3.0[−21]	2.7[−22]
3500	10.1±2.0	1.7[−21]	1.7[−22]

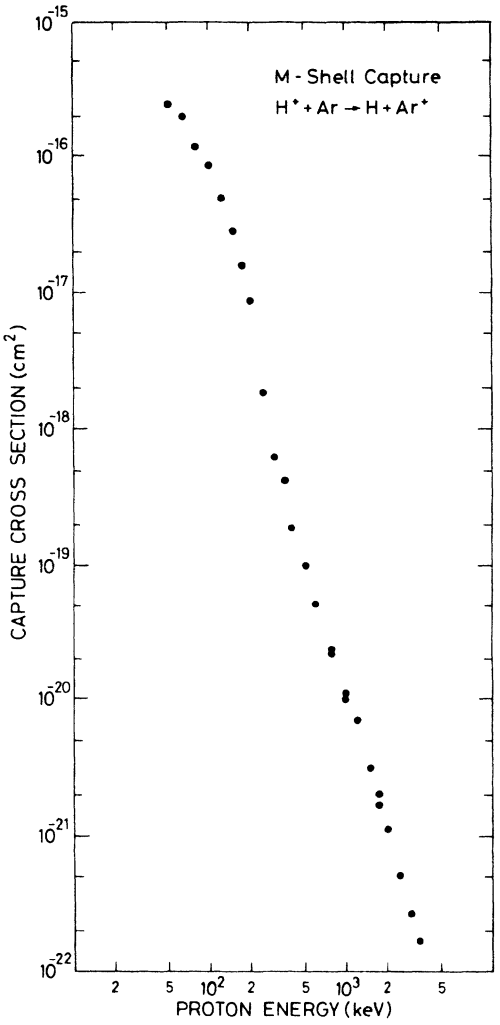

FIG. 5. Energy dependence of M-shell-capture cross sections for protons obtained from the fraction of singly charged recoil ions and published total-capture cross sections (Table I).

gles recoil charge-state distributions by forming the ratio between the fractions of doubly and singly charged ions. The probability is rather constant, about 5%, in the present energy range (800–3500 keV). Neither one of these two effects can account for the structure in the M-shell-capture cross section mentioned earlier, but they probably have the effect of lowering the conditional M-shell cross section measured here by 15–20 % relative to the unconditional cross section. It should also be mentioned that the measured cross sections include capture to all states of the projectile. Theoretical arguments[11] supported by measurements at intermediate energies[12,13] indicate that capture into the ground state accounts for more than 80% of the total cross section for fast protons.

The measured fractions of singly charged recoil ions, the M-shell-capture cross sections, as well as the total cross sections used in deriving the M-shell cross sections, are listed in Table I. The M-shell cross section is displayed as a function of energy in Fig. 5. Due to the strong overall variation of the cross section with energy, the structure around 500 keV may not seem to be very pronounced. The structure is seen more clearly in Fig. 6, where the cross section multiplied by energy to the (arbitrary) power 3.75 is plotted.

We suggest that the above structure can be explained as a combined effect of two radial nodes in momentum wave functions. One of these is the low-momentum node of the Ar(3s) wave function, and the other one is the single node of the Ar(3p) wave function. To qualitatively understand this, it is sufficient to examine the simple OBK approximation[11] for capture into a final state of principal quantum number n by a bare ion of atomic number z. In this approximation, the cross section σ in atomic units is given by[11]

$$\sigma(v)=\frac{1}{8\pi v^2}\int_{p_m}^{\infty}\left[p^2+\left[\frac{z}{n}\right]^2\right]^2|\psi_i(q)|^2|\psi_f(p)|^2 p\,dp\ ,$$

where v is the collision velocity, ψ_i and ψ_f the initial and final wave functions in momentum space, respectively, and p_m the minimum momentum transfer given by

$$p_m=\frac{v}{2}+\frac{\Delta E}{v},$$

where ΔE is the energy defect in atomic units. The variables p and q are related to each other by

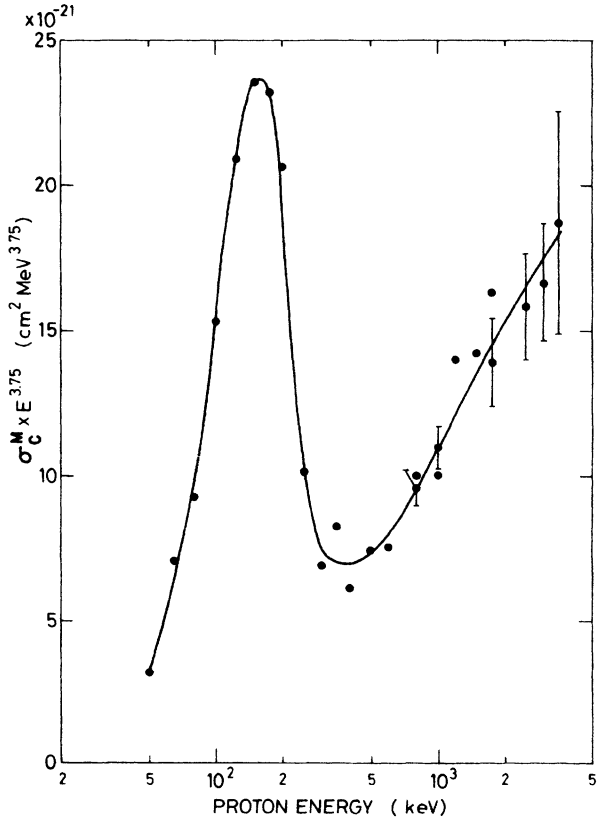

FIG. 6. The cross sections shown in Fig. 5 multiplied by energy to the arbitrary power 3.75 to bring out the structure at 500 keV more clearly.

$$p^2-q^2=2\Delta E \ .$$

The value of q for $p=p_m$ is

$$q_m=\frac{v}{2}-\frac{\Delta E}{v} \ .$$

If the integrand is equal to zero at the lower integration limit p_m because either $\psi_i(q_m)$ or $\psi_f(p_m)$ is zero, then the function $v^2\sigma(v)$ is stationary at the corresponding velocity $v_m=p_m+q_m$, and the cross section varies like v^{-2} at v_m.

In the present case, where an electron is captured (predominantly) to the ground state of H, there are no nodes in the final state, but both initial states belonging to the Ar M shell ($3s$ and $3p$) have nodes. The position of these nodes may be extracted from tables[14] of Compton profiles $J(Q)$ for the initial states,

$$J(Q)=\tfrac{1}{2}\int_Q^\infty |\psi_i(q)|^2 q\, dq \ ,$$

because the Compton profile, just like the function $v^2\sigma(v)$, is stationary at the nodes.

In Table II, we list for the $3s$ and $3p$ states of Ar the momenta Q, at which $J(Q)$ is stationary. These momenta are equal to the momenta q_m. The corresponding velocities v_m and proton energies are also listed. The functions $v^2\sigma(v)$ and $J(Q)$ behave qualitatively in the same way near v_m and q_m, respectively. The function $J(Q)$ decreases rapidly on both sides of the stationary points at q_m. The same is true for the function $v^2\sigma(v)$ near v_m. The cross section $\sigma(v)$ therefore varies like v^{-2} at v_m, as mentioned above, but it decreases much faster at velocities just above or below this velocity.

A close inspection of the high-energy part of the cross section (Fig. 5) shows that it decreases steeply at energies up to 400 keV; it then decreases more slowly in the intermediate interval 500–1500 keV, and finally beyond 2000 keV, it decreases again more strongly. The intermediate interval, where the rapid decrease is diminished, is in good agreement with the interval from 530 to 1450 keV defined by the low-momentum node of the $3s$ wave function and the single node of the $3p$ wave function (Table II). The cross section decreases approximately as E^{-3} in the interval 500–1500 keV which is clearly stronger than the predicted E^{-1} for capture from a specific state near a node. This may be understood as being due to the summation of two cross sections, one of which is decreasing strongly (off the node) in the region where the other decreases more slowly (near the node).

The cross sections for the reactions $H^+ + He \rightarrow H + He^+$ and $H^+ + Ne \rightarrow H + Ne^+$ do not show structure in the energy dependence.[1] The initial $1s$ state of He has no nodes, and the single node of the $2s$ state of Ne lies at a relatively high momentum,[14] so a structure from this node is expected to occur only at about 1900 keV, which is at the upper limit for the experimental measurements.[9] These findings are therefore consistent with our explanation for the structure seen in Ar. The cross section for the reaction $H^+ + Kr \rightarrow H + Kr^+$ shows a structure in the energy dependence which is very similar to that found for $H^+ + Ar \rightarrow H + Ar^+$, but the structure is possibly shifted downwards in projectile energy by about 100 keV compared to Ar. The cross sections for capture from Kr($4s$) and Kr($4p$) are expected to show structures at 410 and 680 keV, respectively.[14] The structure seen in Kr is therefore also attributed to nodes in the initial states.

In semiclassical theories of charge transfer, radial nodes of the initial wave function reveal themselves as minima in the impact-parameter-dependent probabilities. In the simple OBK approximation, the probability is zero at the minima. The probability for electron capture by protons from the L_1 subshell of Ar calculated in the much more complete impulse approximation[15] is never exactly zero, but it shows a distinct minimum associated with the single radial node of the $2s$ wave function. This indicates that the structures in total charge-transfer cross sections, which we have associated with radial nodes on the basis of the OBK approximation, will in general be seen also in more reliable theories, although the effects may be less dramatic.

According to the OBK approximation, the capture cross section shows structure when the collision velocity goes through a characteristic value, at which either the minimum momentum transfer p_m equals the orbital momentum at a node in the momentum-space wave function of the final state, or the momentum absorbed by the target nucleus q equals the momentum at a node of the initial-state wave function. However, in some cases, the range of values covered by q or p_m when v is varied does not include the nodes of the initial or final states. In this situation, no structure should be seen, in spite of the presence of nodes in the wave function. As an example, electron capture into excited states by fast protons in He falls into this category ($\Delta E=0.85$ a.u. for capture to the $3s$ state, $p_m \geq \sqrt{2\Delta E}=1.30$ a.u., and the momenta at the nodes are 0.19 and 0.58 a.u.). Extensive measurements[12,13] of cross sections for capture by fast protons to excited states with radial nodes do not, in fact, show any sign of structure.

Structures in total inelastic cross sections have previously been seen and convincingly explained in terms of nodes in the initial wave functions.[16–18] These cross sections are L_1-subshell ionization cross sections for relatively slow protons. They may at first seem quite different from the present capture cross sections for fast

TABLE II. For the $3s$ and $3p$ states of Ar, we list the positions q_m of the nodes in the momentum-space wave functions (Ref. 14), the energy defects ΔE for capture to the $1s$ state of H, the minimum momentum transfer p_m corresponding to q_m, the velocity v_m corresponding to p_m, and the proton energy corresponding to v_m.

Parameter	$3s$		$3p$
$Q=q_m$	2.2	9.5	3.8
ΔE	0.575	0.575	0.081
p_m	2.4	9.6	3.8
v_m	4.6	19.1	7.6
T (keV)	530	9080	1450

protons, but a closer look shows that the mechanisms leading to the observed structures are essentially the same in the two cases. The ionization process is well described by the first Born approximation which in the full quantal version takes on a form[19] similar to that found in the OBK approximation. The cross section is given as a weighted integral over the initial and final momentum-space wave functions from a lower to an upper limit which may be taken to be infinity. The lower limit, which is weighted strongly by the integrand, is given by the minimum momentum transfer $p_m = I/v$, where I is the ionization potential and v is the projectile velocity. As v is increased, p_m decreases, and the cross section increases. When p_m equals the momentum at a node of the momentum-space initial wave function, the cross section is nearly stationary, and a structure results. This explanation is essentially identical to that given for capture.

IV. SUMMARY

Previously published data from this laboratory on recoil-ion charge-state distributions resulting from single-electron capture by protons in noble gases have been converted by DuBois and Manson[1] into partial cross sections for the different charge states. In doing so, DuBois and Manson discovered a sudden change in the rate of decrease at high energies of the partial cross section for producing singly charged recoils for Ar and Kr targets. Such a phenomenon was not observed for He and Ne.

The present measurements confirm the previous data for Ar and extend them towards higher energies. An analysis based on the OBK approximation suggests that the observed changes in energy dependence are caused by radial nodes in the initial momentum-space wave functions.

*Permanent address: Kansas State University, Manhattan, KS 66506.

[1]R. D. DuBois and S. T. Manson, Phys. Rev. A **35**, 2007 (1987).
[2]M. Rødbro, E. Horsdal-Pedersen, C. L. Cocke, and J. R. Macdonald, Phys. Rev. A **19**, 1936 (1979).
[3]A. Langenberg, F. J. de Heer, and J. Van Eck, in *Abstracts of the IXth International Conference on the Physics of Electronic and Atomic Collisions, Seattle, 1975,* edited by J. S. Risley and R. Geballe (University of Washington, Seattle, 1975), p. 935.
[4]M. H. Chen and B. Crasemann, Phys. Rev. A **10**, 2232 (1975).
[5]V. S. Nikolaev, Zh. Eksp. Teor. Fiz. **51**, 1263 (1966) [Sov. Phys.—JETP **24**, 847 (1967)].
[6]D. R. Bates and R. A. Mapleton, Proc. Phys. Soc. **90**, 909 (1967).
[7]J. K. M. Eichler, Phys. Rev. A **23**, 498 (1981).
[8]K. Omidvar, Phys. Rev. **153**, 121 (1967).
[9]E. Horsdal-Pedersen and L. Larsen, J. Phys. B **12**, 4085 (1979).
[10]H. Tawara and A. Russek, Rev. Mod. Phys. **45**, 178 (1973).
[11]M. R. C. McDowell and J. P. Coleman, *Introduction to the Theory of Ion-Atom Collisions* (North-Holland, Amsterdam, 1970), Chap. 8.
[12]R. H. Hughes, C. A. Stigers, B. M. Doughty, and E. D. Stokes, Phys. Rev. A **1**, 1424 (1970).
[13]J. C. Ford and E. W. Thomas, Phys. Rev. A **5**, 1694 (1972).
[14]F. Biggs, L. B. Mendelsohn, and J. B. Mann, At. Data Nucl. Data Tables **16**, 201 (1975).
[15]D. H. Jakubassa-Amundsen, J. Phys. B **14**, 2647 (1981).
[16]S. Datz, J. L. Duggan, L. C. Feldman, E. Lægsgaard, and J. U. Andersen, Phys. Rev. A **9**, 192 (1974).
[17]C. N. Chang, J. F. Morgan, and S. L. Blatt, Phys. Rev. A **11**, 607 (1975).
[18]C. V. Barros Leite, N. V. de Castro Faria, and A. G. de Pinho, Phys. Rev. A **15**, 943 (1977).
[19]E. Merzbacher and H. W. Lewis in *Corpuscles and Radiation in Matter II,* Vol. 34 of *Handbuch der Physik,* edited by S. Flügge (Springer-Verlag, Berlin, 1958), p. 166.